Advances in Aircraft and Spacecraft Science, *Vol. 6, No. 6 (2019) 515-528*
DOI: https://doi.org/10.12989/aas.2019.6.6.515

Wavenumber analyses of panel vibrations induced by transonic wall-bounded jet flow from an upstream high aspect ratio rectangular nozzle

Stephen A. Hambric*, Matthew D. Shaw and Robert L. Campbell

Applied Research Lab, Penn State University, PO Box 30, State College, PA 16804, U.S.A.

(Received August 20, 2018, Revised December 17, 2018, Accepted January 28, 2019)

Abstract. The structural vibrations of a flat plate induced by fluctuating wall pressures within wall-bounded transonic jet flow downstream of a high-aspect ratio rectangular nozzle are simulated. The wall pressures are calculated using Hybrid RANS/LES CFD, where LES models the large-scale turbulence in the shear layers downstream of the nozzle. The structural vibrations are computed using modes from a finite element model and a time-domain forced response calculation methodology. At low flow speeds, the convecting turbulence in the shear layers loads the plate in a manner similar to that of turbulent boundary layer flow. However, at high nozzle pressure ratio discharge conditions the flow over the panel becomes transonic, and the shear layer turbulence scatters from shock cells just downstream of the nozzle, generating backward traveling low frequency surface pressure loads that also drive the plate. The structural mode shapes and subsonic and transonic surface pressure fields are transformed to wavenumber space to better understand the nature of the loading distributions and individual modal responses. Modes with wavenumber distributions which align well with those of the pressure field respond strongly. Negative wavenumber loading components are clearly visible in the transforms of the supersonic flow wall pressures near the nozzle, indicating backward propagating pressure fields. In those cases the modal joint acceptances include significant contributions from negative wavenumber terms.

Keywords: wavenumber analysis; transonic jet; wall pressure fluctuations; structural vibration; nozzle

1. Introduction

The wall-bounded jet discharge flow from an embedded aircraft propulsion system such as the one shown in Fig. 1 'washes' over the downstream aft deck. At high nozzle pressure ratios, the jet discharge flow is transonic (supersonic just downstream of the nozzle and transitioning to subsonic further downstream as it diffuses) and highly turbulent, inducing strong structural vibration and alternating stresses in the deck structure. Alternating stresses that exceed allowable material limits can cause fatigue cracking and failure.

The vibration response of plates driven by surface pressure fluctuations beneath spatially homogeneous subsonic TBL flow has been studied extensively (see citations in Hambric, Hwang, and Bonness (2004)). Supersonic homogeneous TBL flow has also been studied (see Maestrello (1969), Coe and Chyu (1972), Beresh *et al.* (2011), and Bernardini and Pirozzoli (2011)).

*Corresponding author, Ph.D., E-mail: sah19@arl.psu.edu

http://www.techno-press.org/?journal=aas&subpage=7 ISSN: 2287-528X (Print), 2287-5271 (Online)

However, insufficient attention has been given to spatially inhomogeneous transonic flow excitation of structures, such as those just downstream of embedded jet nozzles on high-speed aircraft. Willis, Schoenster, and Mixson (1978) showed that measured wall pressures on flaps downstream of rectangular and 'D-shaped' nozzles increase with distance from the nozzle. These measurements were limited to subsonic Mach Numbers. Behrouzi and McGuirk (2015) measured the shapes of supersonic jet plumes issuing from various aspect ratio rectangular nozzles with and without downstream decks using Schlieren visualization. Not surprisingly, the presence of the deck strongly impacts the flow field, inducing additional shock cell spatial variability along the deck width. Static surface pressure distributions show the shock cell effects shifting further downstream with increasing nozzle pressure ratio.

The jet flow washing over a downstream panel includes the usual convecting turbulent eddies (most prominently in the shear layer originating from the top lip of the nozzle), but the core flow contains shock cells which interact with the convecting turbulence to form forward and backward propagating pressure pulsations which also excite the underlying structure. The combination of convecting and scattered wall pressure sources in supersonic jet wash excitation is much more complex than the simpler homogeneous TBL wall pressure field, with uncertain interaction of the wall pressures with structural modes. An important and unresolved question is the relative importance of the jet shear layer turbulence-shock cell interaction terms near the discharge compared to the traditional downstream convective excitation components. We explored this subject previously in (Shaw 2015 and Hambric, Shaw, and Campbell 2018) with a converging-diverging rectangular nozzle (8:1 ratio) discharge flow excitation of a downstream flat rectangular plate (see Fig. 2).

In those studies, CFD Hybrid RANS/Large Eddy Simulation (LES) analyses of the wall pressure fluctuations downstream of the nozzle discharge for subsonic and on-design supersonic discharge flow (computed by Low, Bush, and Winkler, 2016) were applied to a finite element model of a structural panel, and time histories and frequency spectra were computed using a modal summation approach. The pressure and vibration calculations were compared to measurements made at the United Technologies Research Center (UTRC) (Winkler *et al.* 2016, Homma *et al.* 2016) to confirm the reasonableness of the simulation procedures. The forced response analysis results were transformed to wavenumber space to determine the relative importance of the convecting and backward propagating surface loading. Filtering the negative wavenumber components from the loading and recomputing the structural response showed that the backward traveling loading is responsible for about 12% of the overall structural vibration at on-design transonic conditions, and a negligible amount at subsonic conditions. The phenomenon of backward propagating wall loading has also been observed by Yang, Palodichuk, Murray, and Jansen (2017) in the expansion region of transonic flow past an angled ramp.

In this follow-up paper, we further examine the wavenumber transforms of the surface loading and structural response to explore the interaction between wall-bounded transonic jet flow excitation and structural panel modes.

2. Analysis approach

A converging-diverging round-to-rectangular nozzle with 8:1 aspect ratio and downstream plate structure are shown in Fig. 2. Also shown in Fig. 2 is an image of the density gradient at the wall computed using CFD analysis at on-design nozzle conditions. Shock cells are clearly visible

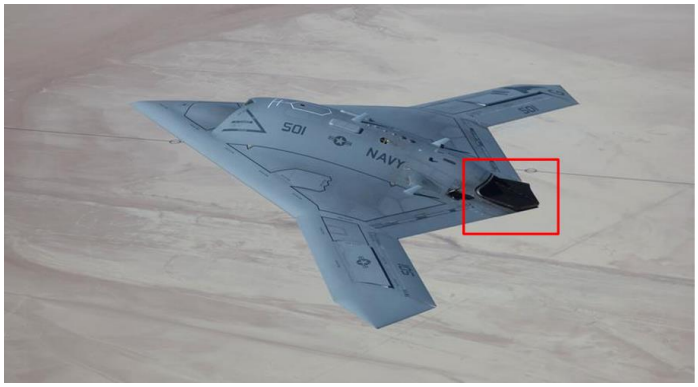

Fig. 1 Aircraft with embedded jet propulsion system and downstream 'deck'

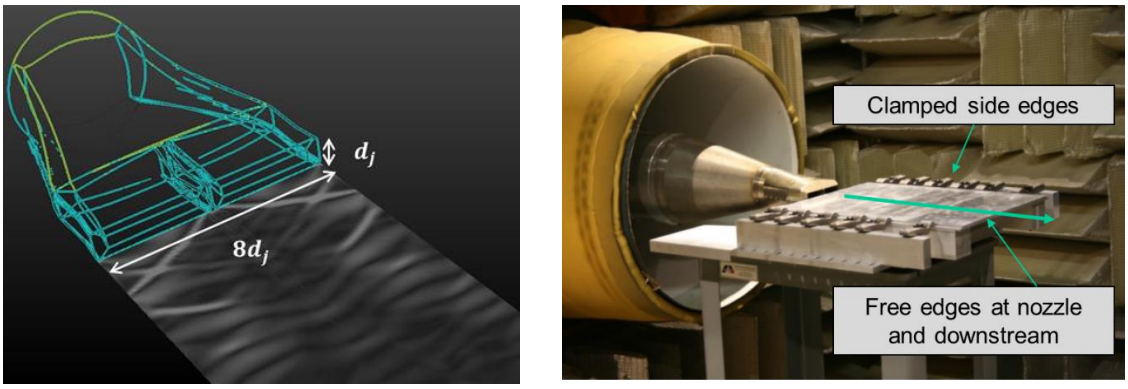

Fig. 2 Nozzle and flow-excited panel

(the lighter sections) in the CFD wall solution. A vertical septum subdivides the discharge nozzle into two 4:1 aspect ratio sections, leading to shock cell patterns symmetric about the nozzle center (this feature is not typical of jet flows described in existing literature). More details on the test hardware and facility at UTRC are in Paterson, *et al.*, (1973) and Winkler, *et al.*, (2016). In this paper, we nondimensionalize the nozzle and plate hardware with the nozzle height d_j.

Converging-diverging nozzle discharge flow varies significantly with nozzle pressure ratio (NPR). Low NPR conditions lead to subsonic jet discharge flow. As operating pressure increases, the supersonic portion of the jet flow moves downstream of the nozzle discharge, leading to shock cell formation and a transonic flow field over the downstream panel. At on-design NPR for the rectangular nozzle studied here, there are several downstream shock cells as shown in the image in Fig. 2. As NPR further increases, the discharge flow becomes 'underexpanded', with stronger shock cells extending further downstream. For wall-bounded jets, the shocks and expansions reflect off the bottom surface, leading to more complex interactions with the shear layer flows emanating from the nozzle walls and with the TBL flow on the bottom surface.

A flat rectangular Aluminum plate with aspect ratio of a/b=0.845 (where a is length and b is width, and h/d_j=0.22, where h is thickness) is directly downstream of the nozzle. The test plate is wider than the nozzle discharge (19.55d_j), and extends 16.52d_j downstream. The edges adjacent to

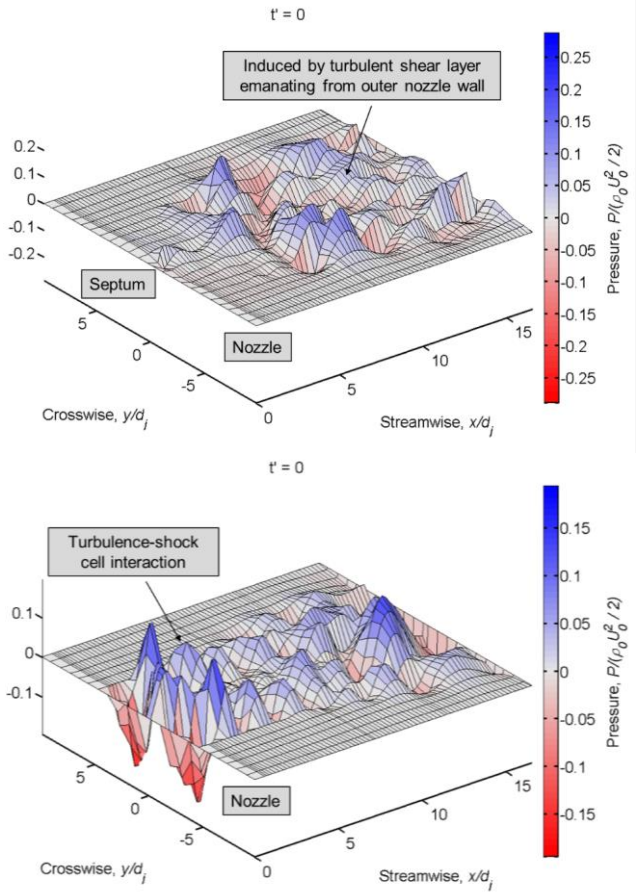

Fig. 3 Snapshots of surface pressures. Top: subsonic flow; Bottom: on-design transonic flow. Septum is located at $y/d_j = 0$

the nozzle and downstream are free, and the edges along the sides in the direction of flow are approximately clamped with a series of screws. A baffle extends around the sides and past the downstream edge (a total surface size of $33d_j$ long and $26d_j$ wide), so that only wall-bounded surface pressures generated by the exhausting jet excite the structure. Simulations and measurements of the flow and structural response were computed for three conditions: subsonic (NPR of 1.6, roughly 50% lower than on-design flow rate), on-design (NPR of 2.62), and underexpanded (NPR of 4.0, roughly 50% higher than on-design flow rate). We consider the subsonic and on-design conditions here; for details on the underexpanded conditions, see the thesis by Shaw (2015).

Images of the CFD simulated wall pressures on the panel and surrounding baffle are shown for the subsonic and on-design conditions in Fig. 3. The CFD calculations were performed with a hybrid compressible RANS/LES method (see Low, Bush, and Winkler (2016)), with LES resolving the large turbulence scales over space and time, and RANS modelling the time-averaged flow and turbulence in the small scales within the bottom surface boundary layer and in the initial regions of the developing shear layers. All time-varying forcing of the panel in the CFD

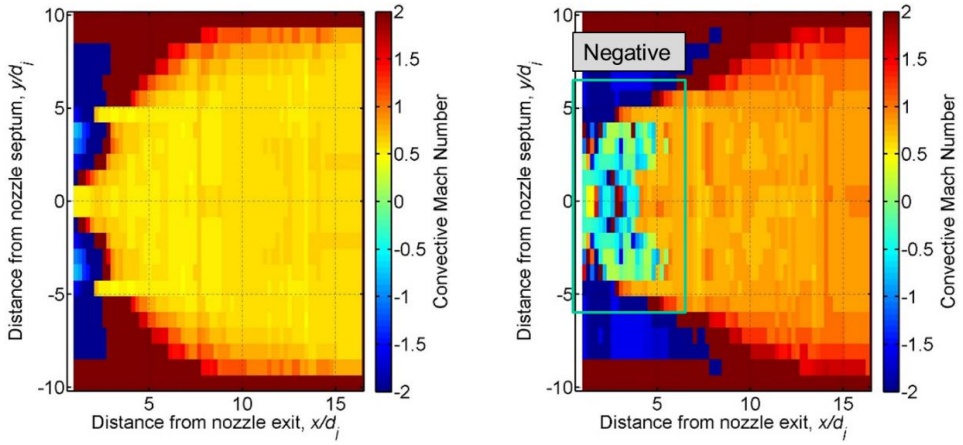

Fig. 4 Convective velocities normalized by mean sound speed based on spatial correlation analysis of pressure time histories. Left: subsonic flow; Right: on-design transonic flow. The dark red and dark blue regions for $|y/d| > 5$ and $x/d < 7$ indicate regions where convective velocities could not be accurately computed. The septum is located at y/d_j of 0

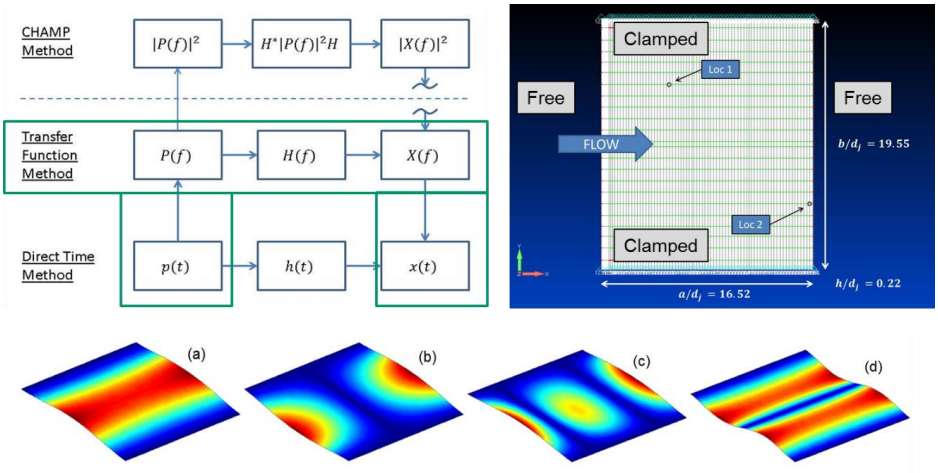

Fig. 5 Analysis approaches (upper left), FE model (upper right), and first four modes of panel (bottom)

simulations is caused therefore by large-scale turbulence in the shear layers and its scattering due to interactions with the shock cells.

The CFD grid is described by Low in detail, and extends 10 nozzle heights upstream of the exhaust plane and 64 nozzle heights downstream. Domain inlet boundary conditions were specified as uniform flow and pressure, with a constant static pressure applied at the domain discharge. The inlet and outlet conditions were tuned to adjust the flow rates to the three targeted nozzle pressure ratios. 'Bulk' flow Mach Numbers may be calculated for each NPR using standard fluid mechanics relations for isentropic flow (see Appendix G of Shaw (2015)). For the NPRs studied here, the bulk Mach Numbers are 0.85 (subsonic), 1.26 (on-design), and 1.56 (underexpanded). Of course, there are significant flow and sound speed variations within the nozzle flow field.

Animations of the wall pressure distributions for all three conditions are available in Appendix G of Shaw (2015). The subsonic wall pressures resemble those of TBL flow, but are in fact caused by the turbulence in the shear layer generated by flow discharging over the top lip of the nozzle. The transonic wall pressures show convection downstream of the nozzle, but also show strong shock cells near the nozzle discharge. The shock cells scatter the shear layer turbulence in all directions, including backwards against the mean flow. Fig. 4 shows the effective velocities of the structural excitation estimated from the space-time correlations of the surface pressures. The velocities are normalized by the mean sound speed of the discharge flow (computed using the isentropic flow equations). For subsonic flows, all excitation velocities are positive, and are about 60% of the mean sound speed. For on-design transonic flows, however, negative excitation velocities are evident near the shock cells, along with faster positive convection velocities further downstream. The effects of these backward propagating loading terms on structural mode response are investigated here.

A finite element model was constructed of the structure using NASTRAN thick plate elements, as shown in Fig. 5. The nodal spacing is coincident with the grid used in the CFD simulations so that wall pressure time histories could be applied directly to the FE model without spatial interpolation. The leading and trailing edges of the plate are free, and the streamwise edges are clamped. Using the commercial FE solver NX NASTRAN, the mass-normalized mode shapes and resonance frequencies of the plate were calculated. The first four mode shapes are also shown in Fig. 5: the (0, 1), (1, 1), (2, 1), and (0, 2) modes, where the modes are numbered with the ordered pairs (m, n), where m and n represent the number of half wavelengths in the flow and cross-flow directions, respectively.

Fig. 5 also shows a flow chart of various methods that may be used to analyze structural response in the time or frequency domains. For simple forced vibration response to statistically stationary and ergodic forces, the frequency domain method (denoted 'CHAMP') is most efficient, and is well established in the literature (see Hambric, Hwang, and Bonness (2004) for details). In this application, however, alternating stresses and their impact on fatigue were required, such that peak events over time were necessary. The traditional time domain forced vibration analysis method requires significant computational resources, and can induce artificial peaks due to initial transients in the numerical integration response. Instead, the transfer function method is applied, where the loading time histories are Fourier transformed to complex frequency space, and multiplied by the complex frequency response functions generated via summation of the FE modes. The response is inverse transformed back to the time domain. The transfer function method is significantly more computationally efficient than the traditional time-domain approach, and avoids contamination of the response time history by initial transients. For more details on the methods, see Hambric, Shaw, and Campbell (2018) and Shaw (2015).

Modes through order (5,3) were included in the modal summation, with the maximum resonance frequency about twice that of the upper range of the frequency response. The surface loading time history was limited by computational resources, and extends to about 6000 tU_o/d_j with a sampling frequency about 5 times that of the upper frequency of the analysis (the actual sampling frequency in the CFD analyses is much higher to maintain accurate calculations over time; the data are downsampled for the forced response analyses). The relatively short time history leads to visible random error in the resulting spectra, which is evident in the forthcoming plots. In contrast, the measured time histories are about 50 times longer than those computed by CFD, resulting in reduced random error and smoother spectra.

3. Results

3.1 Measured and simulated structural vibrations

Fig. 6 compares simulated and measured structural displacement power spectral densities (PSDs) at a point on the plate computed from the response time histories for subsonic and on-design transonic flow conditions. The PSDs are non-dimensionalized against flow and structural parameters. Since integral length scales are not well defined and are inhomogeneous over the plate surface, no attempt is made to include them in the non-dimensionalization. Instead, an additional plate area term is used. Frequency is nondimensionalized against nozzle height and bulk flow velocity. The simulations and measurements agree reasonably well, with some discrepancies due to inconsistencies between actual and simulated resonance frequencies and damping loss factors. The random error in the simulated spectra is due to the short loading time record length (see above). Several structural modes are annotated in the plots, including the (3,1) and (3,2) modes, which were selected for detailed wavenumber analysis based on their high amplitudes at both flow conditions.

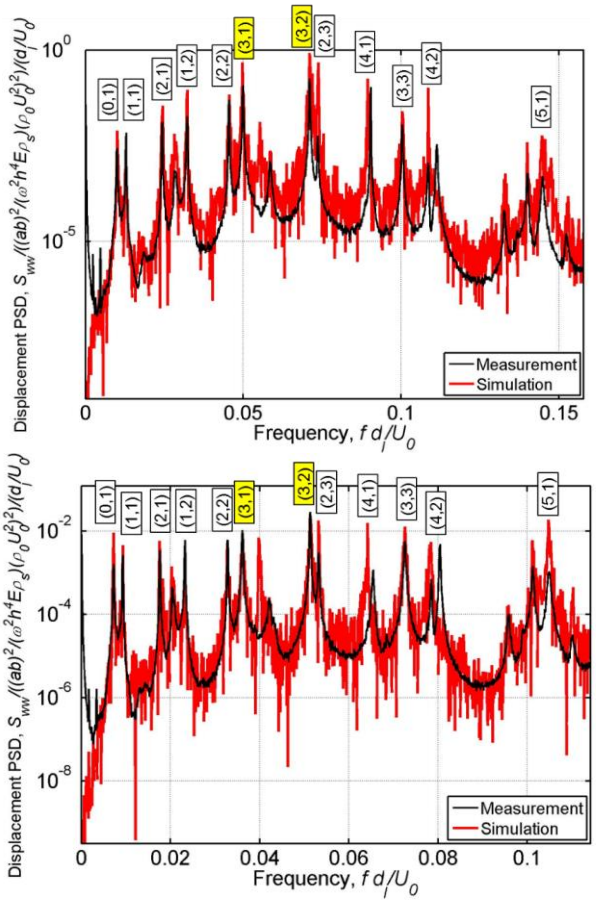

Fig. 6 Nondimensionalized measured and simulated displacement power spectral densities at x/d=5.3 and y/d=4.6. Top: subsonic flow; Bottom: on-design transonic flow

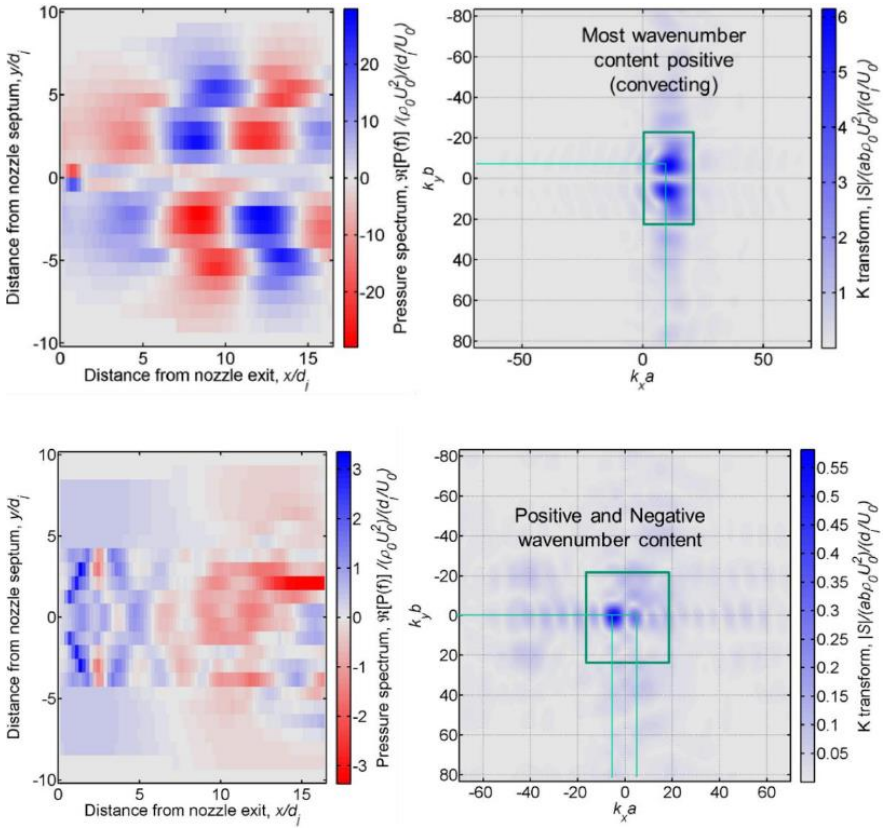

Fig. 7 Spatial distributions of pressure spectra (left) and wavenumber transforms (right). Top: fD/U=0.075 for subsonic flow (corresponding to the resonance frequency of the (3,2) mode); Bottom: fD/U=0.037 for on-design transonic flow (corresponding to the resonance frequency of the (3,1) mode

3.2 Wavenumber transforms and analysis

The spatial distributions of surface loading and structural mode shapes and response were transformed into wavenumber space using

$$S(k_x, k_y, f) = \iint F(x, y, f) e^{ik_x x} e^{ik_y y} dxdy$$

Since the mesh spacing is not uniform, the transformations were performed manually, simply integrating numerically over the plate dimensions using the grid shown in Fig. 5. For general guidance on wavenumber transformations see the tutorial by Hambric and Barnard (2018). Fig. 7 compares spatial distributions of the real part of the pressure cross-spectrum with corresponding wavenumber distributions at frequencies near the (3,1) and (3,2) modes. For subsonic flow at fD/U=0.075 (corresponding to the resonance frequency of the (3,2) mode), nearly all the wavenumber content is positive, representing turbulence convecting in the direction of bulk flow at $k_x a$ of ~3π and $k_y b$ of ~2π (about one and a half wavelengths over the panel length and one wavelength over the width). For on-design transonic flow at fD/U=0.037 (corresponding to the portion of the wavenumber transforms, with peaks at $k_x a$ of ~ +/-π. These peak wavenumber

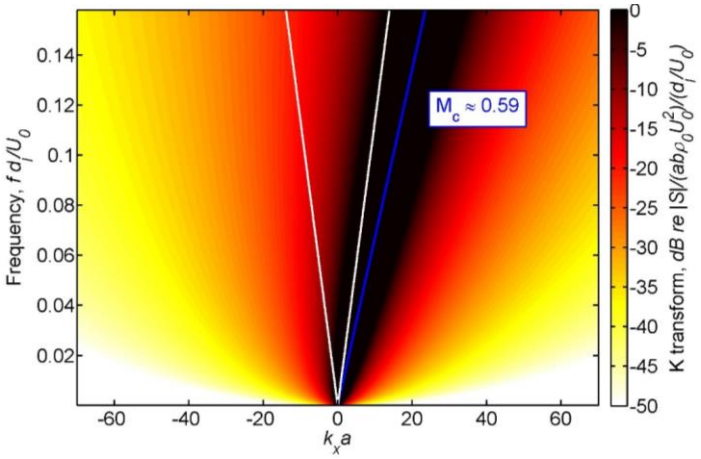

Fig. 8 Streamwise wavenumber content of Corcos model using bulk flow speed for subsonic flow

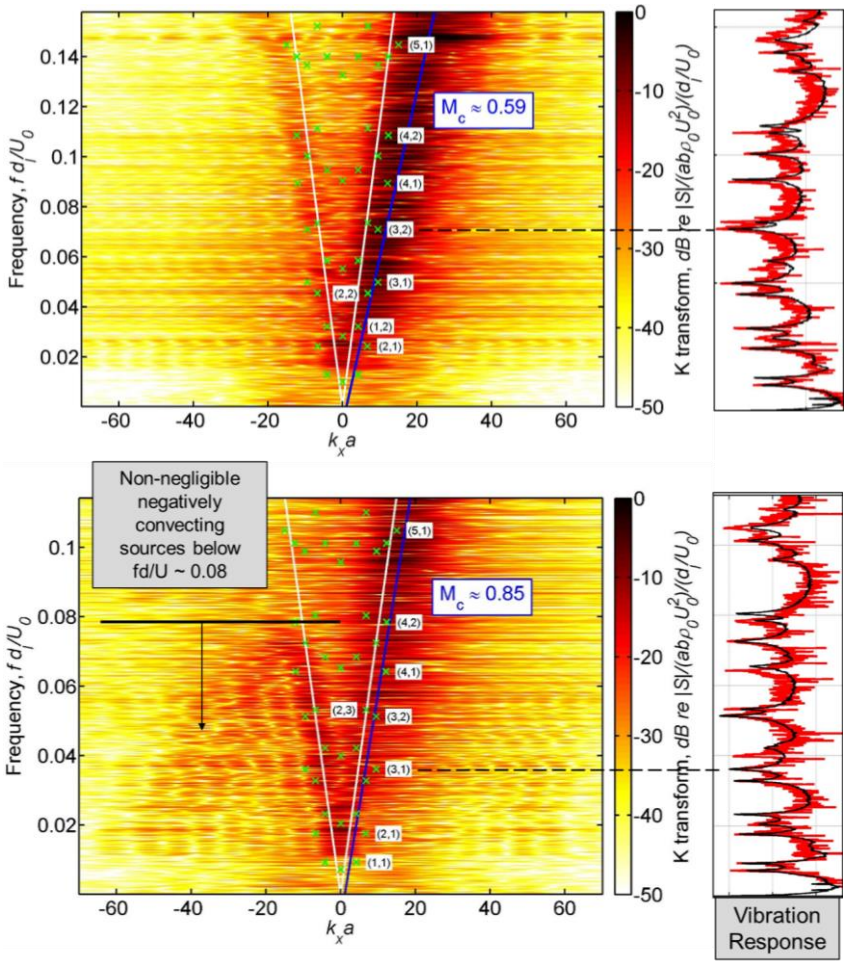

Fig. 9 Wavenumber transforms of surface pressures for *ky*=0 with superimposed modal, convective, and acoustic wavenumbers. Top: subsonic flow; Bottom: on-design transonic flow

content regions dictate which structural modes respond well to the excitation field.

Fig. 8 shows the streamwise (k_x) wavenumber-frequency spectrum for the well-known Corcos model of TBL wall pressure fluctuations (1967)

$$S_{Corcos}(k_x, f) = \frac{2\alpha_x}{\alpha_x^2 + (U_c k_x/\omega - 1)^2}$$

using the subsonic flow bulk velocity and an assumed streamwise decay coefficient α_x of 0.05. Although Corcos postulated this model to simulate homogeneous TBL flow wall pressures, many investigators have used it (sometimes inappropriately), along with empirically determined decay coefficients, to simulate more complex turbulent flow excitation fields. This is because the model incorporates the two main features necessary for modeling convecting turbulence – a convective term ($U_c k_x/\omega$), and exponentially decaying correlations in the flow and cross-flow directions. However, this model is not recommended for simulating the transonic flows studied here, and is shown in this paper only to contrast against simpler TBL flows.

Fig. 9 shows the wavenumber-frequency spectra of the streamwise component of the surface excitation (x-direction) for k_y =0. The subsonic wavenumber distribution is quite similar to that of the Corcos model. Superimposed on the plots are wavenumbers for the mean bulk flow speed ω/U_o (blue – positive only), speed of sound ω/c_o (white – both positive and negative), and selected structural modes at their resonance frequencies (green symbols). Modal wavenumbers near the bulk flow speed wavenumber are annotated, as are the modes with the strongest response (see the right side of the figures). Since the transform is performed over a finite rectangle and the wall pressures are highly inhomogeneous, the resulting wavenumber content is spread over wide ranges. Nevertheless, strong convective energy is evident in the plots. The negative wavenumber content is much stronger for transonic flow, and is centered around the acoustic wavenumber, indicating backscattered sound waves caused by shear layer turbulence interacting with the shock cells near the nozzle discharge.

Figs. 10 and 11 illustrate how the wall pressure field and mode shapes interact in wavenumber space for the (3,1) and (3,2) modes. In both figures, wavenumber transforms of the mode shapes are multiplied by the transforms of the wall pressures at the modal resonance frequencies to show the distribution of the 'joint acceptance', defined by Powell (1958) and used by many investigators since. The mode shape transforms are constant (since they do not change with flow speed), but the excitation transforms vary significantly with flow speed and frequency. In these examples, the strongest excitation wavenumber content is at low wavenumbers, but higher wavenumber content is also evident. The largest differences in the excitation wavenumber content are clearly the negative terms for transonic flow conditions. The modal wavenumber distribution acts as a wavenumber filter when multiplied by the excitation wavenumber field, producing a joint acceptance wavenumber distribution that is either purely positive (for subsonic flow) or both positive and negative (for transonic flow). In these examples, the peak modal wavenumbers dominate the distributed joint acceptance. Integrating over the joint acceptance wavenumber distribution yields the total joint acceptance of the wall pressure field by the mode.

Finally, the wavenumber transforms of the pressure field computed over only the upstream (first half of the plate downstream of the nozzle) and downstream (second half of the plate) sections of the plate are shown in Fig. 12. These 'truncated' transforms clearly show that the negative wavenumber content is concentrated primarily near the nozzle discharge, consistent with the effective velocity distributions shown in Fig. 4.

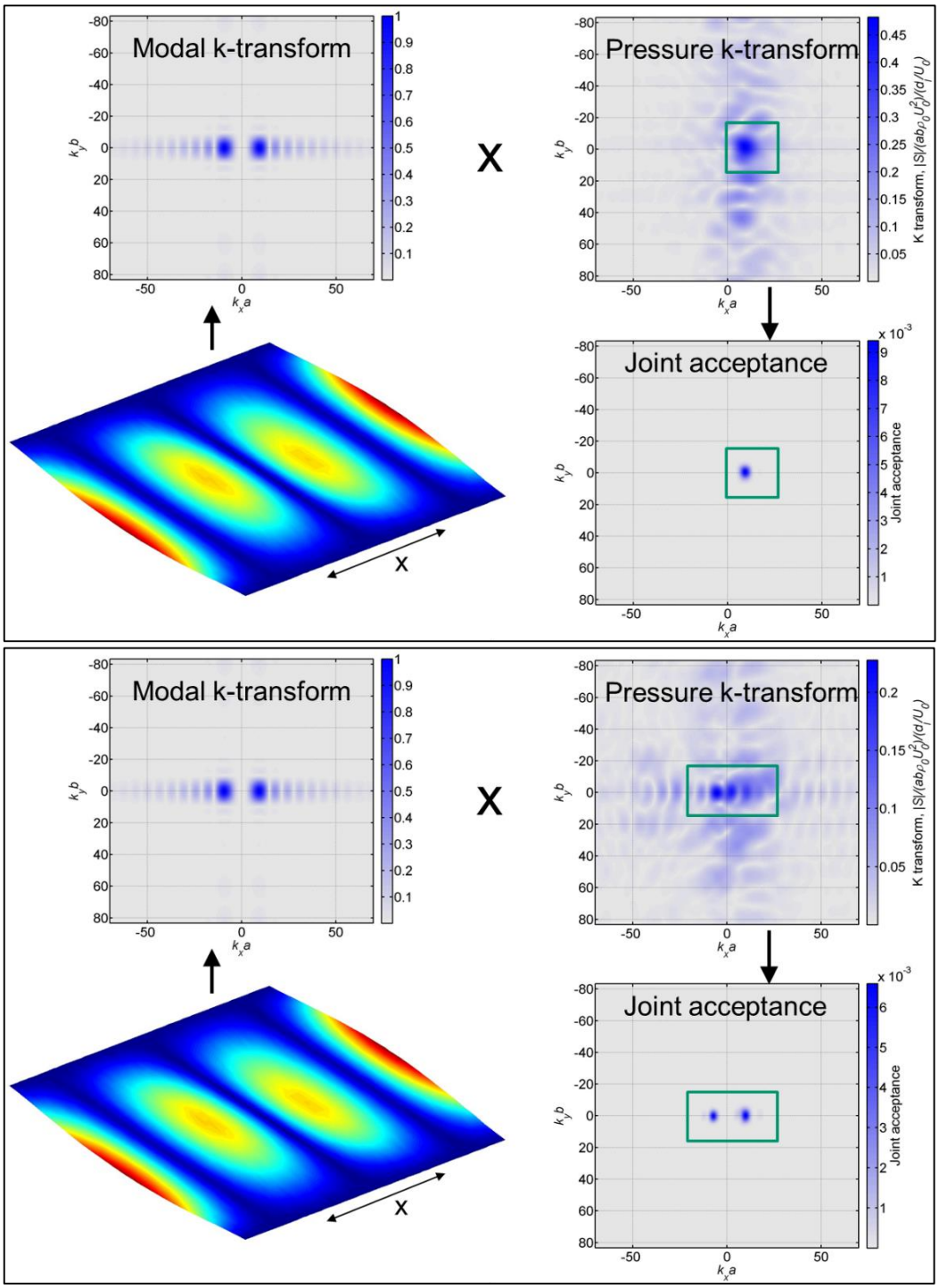

Fig. 10 Wavenumber transforms of (3,1) mode (upper left), pressure excitation at (3,1) mode resonance frequency (upper right), and joint acceptance (lower right). Top: subsonic flow; Bottom: on-design transonic flow

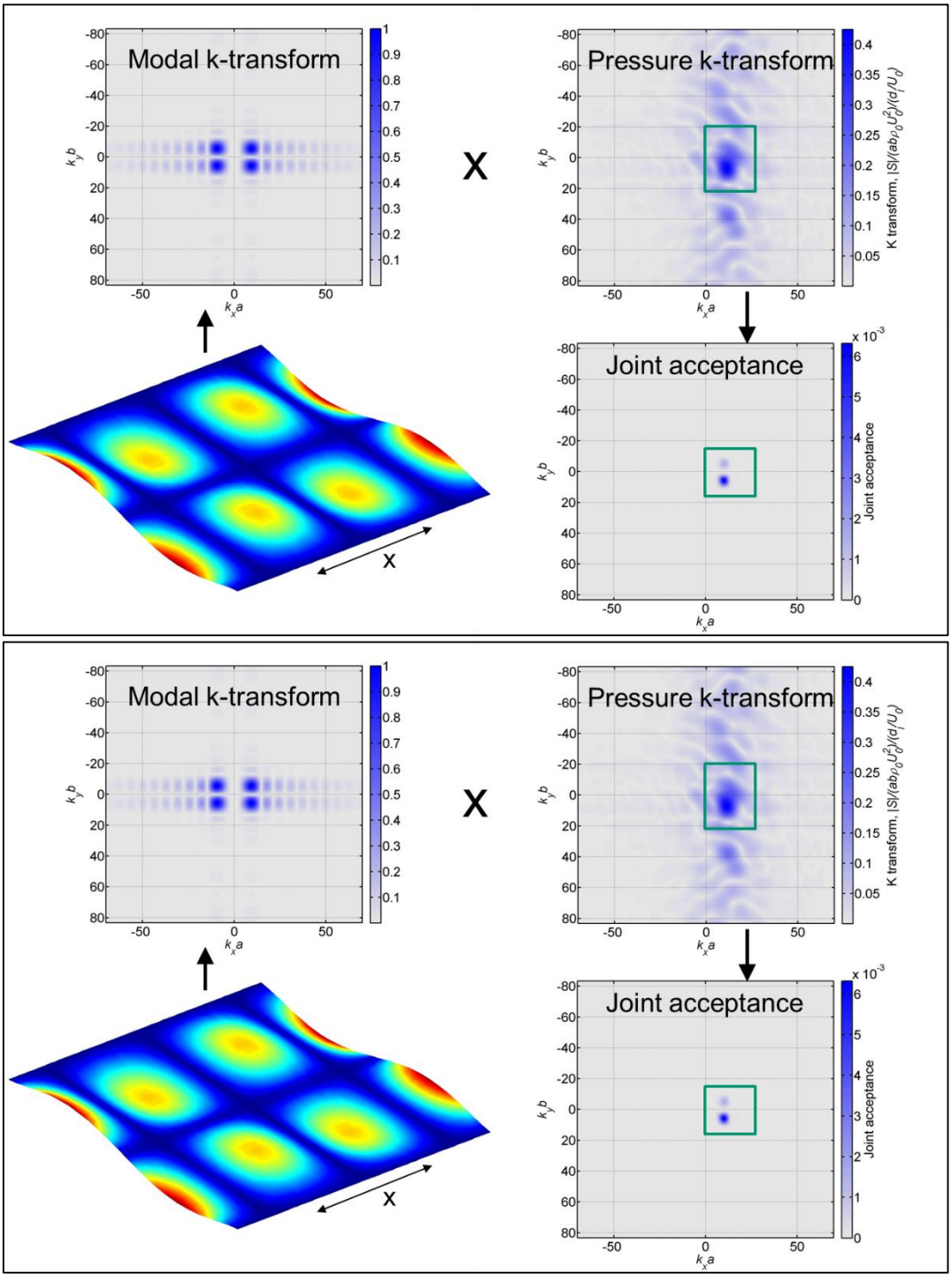

Fig. 11 Wavenumber transforms of (3,2) mode (upper left), pressure excitation at (3,2) mode resonance frequency (upper right), and joint acceptance (lower right). Top: subsonic flow; Bottom: on-design transonic flow

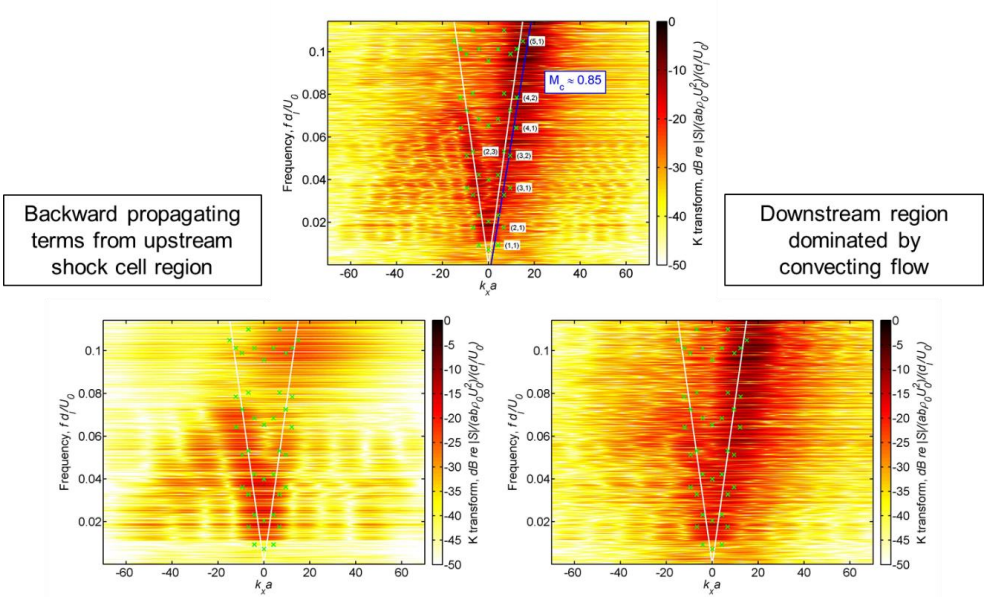

Fig. 12 Total (top), upstream (lower left), and downstream (lower right) wavenumber loading components for on-design transonic flow

4. Conclusions

The panel vibrations induced by wall-bounded jet flow from an upstream high aspect ratio rectangular nozzle have been simulated using CFD Hybrid RANS/LES wall pressures applied to a structural FE model using a transfer function time domain approach. Correlation analysis and wavenumber-based assessments of the wall pressure loading show that strong negative backward traveling components within and between shock cells for on-design operating conditions with transonic discharge flow are important exciters of structural vibration. The negative traveling pressure waves are concentrated near the nozzle discharge, and are caused by interaction between the turbulence in the shear layer and the shock cells, with forward and backward scattered waves loading the surface.

Wavenumber analysis of the wall pressure field and modal response is useful for identifying the causes of peak vibrations. Modes with wavenumber distributions which align with peak loading wavenumber content are strongly excited. The subsonic flow wall pressure field is similar to that of a simple Corcos model, but the transonic flow wall pressure field is more complicated. Backward propagating source terms near the nozzle excite the panel for on-design transonic flows. Examples of two strongly excited modes with modal wavenumbers nearly coincident with excitation wavenumber peaks show the differences in joint modal acceptance for subsonic and transonic flows. The modes act as wavenumber filters around their dominant modal wavenumber peaks, with joint acceptance of subsonic flow limited to positive wavenumbers, and joint acceptance of transonic flows spanning positive and negative wavenumbers.

Acknowledgments

We are grateful to Rick Labelle at Pratt and Whitney for sponsoring this work. We also acknowledge the data provided by Kenji Homma and Robert Schlinker at UTRC, and the helpful

comments and CFD simulations provided by Kerwin Low, Brandon Rapp, and John Liu at Pratt and Whitney. This document is publicly released courtesy of Pratt and Whitney.

References

Behrouzi, P. and McGuirk, J. (2015), "Underexpanded jet development from a rectangular nozzle with Aft-deck", *AIAA J*., **53**(5), 1287-1298. https://doi.org/10.2514/1.J053376.

Beresh, S.J., Henfling, J.F., Spillers, R.W. and Pruett, B.O.M., (2011), "Fluctuating wall pressures measured beneath a supersonic turbulent boundary layer", *Phys. Fluids*, **23**, 07511. https://doi.org/10.1063/1.3609271.

Bernardini, M. and Pirozzoli, S. (2011), "Wall pressure fluctuations beneath supersonic turbulent boundary layers", *Phys. Fluids*, **23**, 085102. https://doi.org/10.1063/1.3622773.

Camussi, R. and DiMarco, A. (2015), *Wall Pressure Fluctuations Induced by Supersonic Turbulent Boundary Layer*, in *Flinovia - Flow Induced Noise and Vibration Issues and Aspects*, Springer.

Coe, C.F. and Chyu, W.J. (1972), "Pressure fluctuation inputs and response of panels underlying attached and separated supersonic turbulent boundary layers", NASA TM X-62, 189.

Corcos, G.M. (1967), "The resolution of turbulent pressures at the wall of a boundary layer", *J. Sound Vib*., **6**(1), 59-70. https://doi.org/10.1016/0022-460X(67)90158-7.

Hambric, S.A. and Barnard, A.R., (2018), "Tutorial on wavenumber transforms of structural vibration fields", *Proceedings of the Internoise 2018*, Chicago, Illinois, U.S.A., August.

Hambric, S.A., Hwang, Y.F. and Bonness, W.K. (2004), "Vibrations of plates with clamped and free edges excited by low-speed turbulent boundary layer flow", *J. Fluids Struct*., **19**(1), 93-110. https://doi.org/10.1016/j.jfluidstructs.2003.09.002.

Hambric, S.A., Shaw, M.D. and Campbell, R.L. (2018), "Panel vibrations induced by supersonic wall-bounded jet flow from an upstream high aspect ratio rectangular nozzle", *Proceedings of the International Conference on Flow Induced Noise and Vibration Issues and Aspects*, State College, Pennsylvania, U.S.A., April.

Homma, K., Branwart, P.R., Schlinker, R.H. and Rapp, B.M. (2016), "Unsteady loading and dynamic response of a structure excited by a high-speed wall-bounded jet, Part II: Structural Response", *Proceedings of the 22nd AIAA/CEAS Aeroacoustics Conference*, Lyon, France, May-June.

Low, K.R., Bush, R.H. and Winkler, J. (2016), "Simulating sources of unsteadiness in a high-speed wall-bounded jet", *Proceedings of the 46th AIAA Fluid Dynamics Conference, AIAA Aviation*, Washington, D.C., U.S.A., June.

Maestrello, L. (1969), "Radiation from and panel response to a supersonic turbulent boundary layer", *J. Sound Vib*., **10**(2), 261-295. https://doi.org/10.1016/0022-460X(69)90200-4.

Paterson, R., Vogt, P. and Foley, W. (1973), "Design and development of the United Aircraft Research Laboratories acoustic research tunnel", *J. Aircraft*, **10**(7), 427-433. https://doi.org/10.2514/3.60243.

Powell, A. (1958), "On the fatigue failure of structures due to vibrations excited by random pressure fields", *J. Acoust. Soc. Am*., **30**(12), 1130-1135. https://doi.org/10.1121/1.1909481.

Shaw, M.D. (2015), "Predicting vibratory stresses from aero-acoustic loads", Ph.D. Dissertation, Penn State University, State College, Pennsylvania, U.S.A.

Winkler, J., Schlinker, R.H., Simonich, J.C. and Low, K.R. (2016), "Unsteady loading and dynamic response of a structure excited by a high-speed wall-bounded jet, Part I: Aerodynamic Excitation", *Proceedings of the 22nd AIAA/CEAS Aeroacoustics Conference*, Lyon, France, May-June.

Yang, M.Y., Palodichuk, M.T., Murray, N.E. and Janson, B.J. (2017), "Prediction of structural response in transonic flow using wavenumber decomposition of fluctuating pressures", *Proceedings of the 23rd AIAA/CEAS Aeroacoustics Conference*, Denver, Colorado, U.S.A., June.

CC